Electronic Supplementary Material (ESI) for Journal of Materials Chemistry A.
This journal is © The Royal Society of Chemistry 2021

Supplementary Information

Hierarchically 3D Nanoporous Structured Co_9S_8@Ni_x:Mo_y-Se Core-shell Nanowire Arrays Electrode for the High-performance Asymmetric Supercapacitor

*JiuYi Dai[a], Soram Bobby Singh [a], Nam Hoon Kim[a] and Joong Hee Lee[a,b]**

[a] Department of Nano Convergence Engineering, Jeonbuk National University, Jeonju, Jeonbuk, 54896, Republic of Korea.

[b] Carbon Composite Research Center, Department of Polymer-Nano Science and Technology, Jeonbuk National University, Jeonju, Jeonbuk, 54896, Republic of Korea.

*Corresponding authors:

Email address: jhl@jbnu.ac.kr (Prof. Joong Hee Lee) Fax: +82 632702341; Tel: +82 632702342

Synthesis of Fe_2O_3@ PANNFs@N-rGO Aerogel:

GO, and PAN Nanofibers(NFs) were synthesized by the previous method [1, 2]. Fe_2O_3@PAN NFs@N-rGO hydrogel was prepared using the following detailed procedure: Briefly, 50 mg GO was dispersed into 10 mL DI water with ultrasonication for 2 h. And 50mg PAN NFs was dispersed into 10 mL DI water with ultrasonication for 2 h. then the GO solution was mixed with PAN NFs solution by stir 30 mins. 0.5mmol $FeCl_3 \cdot 6H_2O$ was dissolved into 5 mL DI water separately. Then, the iron precursor solution and 2 ml $NH_3 \cdot H_2O$ (28%) were added dropwise into the GO and PAN NFs suspension under vigorous stirring. The mixture was vigorously stirred for another 1h at room temperature. Subsequently, the mixture was transferred into a 50 mL Teflon-lined stainless-steel autoclave. The autoclave was sealed, maintained at 180 °C for 12 h, and then slowly cooled down to the room temperature naturally. The black cylinder hydrogel was carefully fetched out and put into DI water to dialyzing for 12 h. After that, the dried Fe_2O_3@PANNFs/N-rGO cylinder hydrogel was obtained by freeze-drying.

Fabrication of aqueous asymmetric supercapacitors (ASCs):

Typically, the aqueous ASC consisted of the NKK TF40 (thickness: 40 μm; Nippon Kodoshi Corporation) as the separator of two pieces of electrode materials (size:10 mm × 10 mm) aqueous 2 M KOH solution as the electrolyte.

In the aqueous ASCs system, the self-supported Fe_2O_3@PANNFs/N-rGO hydrogels were used as the negative materials, and the as-synthesized Co_9S_8@$Ni_{0.5}Mo_{0.5}$-Se NWAs were used as the positive materials. To realize a high electrochemical property for Co_9S_8@$Ni_{0.5}Mo_{0.5}$-Se // Fe_2O_3@PANNFs/N-rGO ASC, we optimized the mass ratio of the Co_9S_8@$Ni_{0.5}Mo_{0.5}$-Se NWAs to Fe_2O_3@PANNFs/N-rGO around~ 0.43 and the working voltage window of the device to ~

1.7 V. The optimal mass ratio of positive materials to negative materials was counted by Equation (5).

Fabrication of solid-state asymmetric supercapacitors:

The electrochemical performance of all-solid-state ASC was measured under a two-electrode system, which included two slices of electrode material with the same size (10 mm × 10 mm), PVA/KOH film as a separator, and KOH/PVA solid-gel as solid-state electrolyte. In the two-electrode system, Co_9S_8@$Ni_{0.5}Mo_{0.5}$-Se NWAs grown 3D porous Ni foam was used as the positive electrode, and Fe_2O_3@PANNFs/N-rGO coated on Ni foam was used as the negative electrode. The KOH/PVA gel electrolyte was prepared using the following procedure: 2 g KOH and 2 g PVA (Mw = 98000) were dissolved in 22 mL DI water and then heated at 95 °C for 2 h under vigorous stirring. The electrodes and separator were soaked in the electrolyte for 10 min. and then allowed to solidify the sample by freeze and unfreeze repeatedly.

Materials characterization

The field-emission scanning electron microscope (FE-SEM; SUPRA 40 VP; Carl Zeiss, Germany) was used to characterize the surface morphology of the as-synthesized materials. The EDAX analysis (SUPRA 40 VP; Carl Zeiss, Germany) was used to investigate the quantity of the elemental composition of the as-obtained materials. The transmission electron microscopy (TEM) and high-resolution TEM (HR-TEM; H-7650; Hitachi Ltd., Japan) were used to examine the intrinsic morphology of the as-synthesized electrode material. The STEM-energy dispersive X-ray spectroscopy (EDS) mapping was used to analyze the elemental distribution of the as-obtained electrode materials. We examined the crystallinity of the as-synthesized materials by X-ray diffraction (XRD) (Rigaku Corporation, Japan, Cu Kα radiation (λ = 0.154

nm)). The theta probe AR-XPS system (Thermo Fisher Scientific, UK) was used to investigate the elemental compositions and valence states of the as-obtained electrode material. The N_2 sorption isotherms analysis was used to measure the SSA and the pore-size distribution of the as-obtained electrode material (at 77K; Micromeritics ASAP 2020).

Electrochemical measurement

The electrochemical workstation (CHI660D, CH Instruments, Inc., USA) was used to study the electrochemical properties of materials under a three-electrode configuration system. The aqueous 2 M KOH solution was used as the electrolyte. In a three-electrode configuration system, the Pt foil was used as counter electrodes, the Ag/AgCl/3.0 mol/kg KCl was used as the reference electrode, and the as-obtained pristine Co_9S_8, Co_9S_8@MoSe, Co_9S_8@$Ni_{0.5}Mo_{0.5}$-Se，Co_9S_8@$Ni_{0.25}Mo_{0.75}$-Se, and Co_9S_8@$Ni_{0.75}Mo_{0.25}$-Se electrodes were directly used as the working electrode. The mass loading for the Co_9S_8, Co_9S_8@$Ni_{0.5}Mo_{0.5}$-Se, Co_9S_8@$Ni_{0.25}Mo_{0.75}$-Se, Co_9S_8@$Ni_{0.75}Mo_{0.25}$-Se, and Co_9S_8@MoSe electrodes are 1.5 mg cm^{-2}, 2.0 mg cm^{-2}, 2.0 mg cm^{-2}, 2.1 mg cm^{-2}, and 2.2 mg cm^{-2}, respectively. The electrochemical impedance spectroscopy (EIS) test was examined by using a 5 mV amplitude with a frequency range from 0.01 Hz to 100 kHz.

Calculations

The areal capacity (C_{ac}, mAh cm^{-2}) and the specific capacity (C_{sc}, mAh g^{-1}) of the as-obtained materials under the three-electrode configuration system and the ASC device were counted from general charge and discharge (GCD) curves using the following Equations Eqs.S (1) and Eqs.S (2) [3,4] :

$$C_{ac} = \frac{2I \times \int Vdt}{AV} \quad (1)$$

$$C_{sc} = \frac{2I \times \int Vdt}{mV} \quad (2)$$

Where the "I" (mA) is the current of the system during the discharge process, the "A" (cm^{-2}) is the area of the active electrode, the "m" (g) is the mass of the active electrode material, and the "∫Vdt" is the absolutely integral area of the GCD curve (discharge process). The energy densities (E, W h kg^{-1}) and the power densities (P, W kg^{-1}) of the assembled ASC device were calculated using the following Equations Eqs.S (3) and Eqs.S (4) [5]:

$$E = \frac{I \times \int Vdt}{m \times 3.6} \quad (3)$$

$$P = \frac{E}{t} \times 3600 \quad (4)$$

Where the "I" (mA) is the current of the ASC device, the "∫Vdt" is the absolutely integral area of the GCD curve (discharge part), the "m" (g) is the mass of the material (active electrode), and "t" is the discharge time. The mass ratio of the Co_9S_8@$Ni_{0.5}Mo_{0.5}$-Se (positive) and Fe_2O_3@PANNFs/N-rGO (negative) materials were counted by Equation Eqs.S(5) [4]:

$$\frac{m_+}{m_-} = \frac{C_- \times V_-}{C_+ \times V_+} \quad (5)$$

where the "m−" is the negative materials mass, the "m+" is the positive materials mass; the "C−" is the specific capacity (negative materials), the "C+" is the specific capacity (positive materials); and "V" is the working voltage widow for the negative (-) and positive (+) materials.

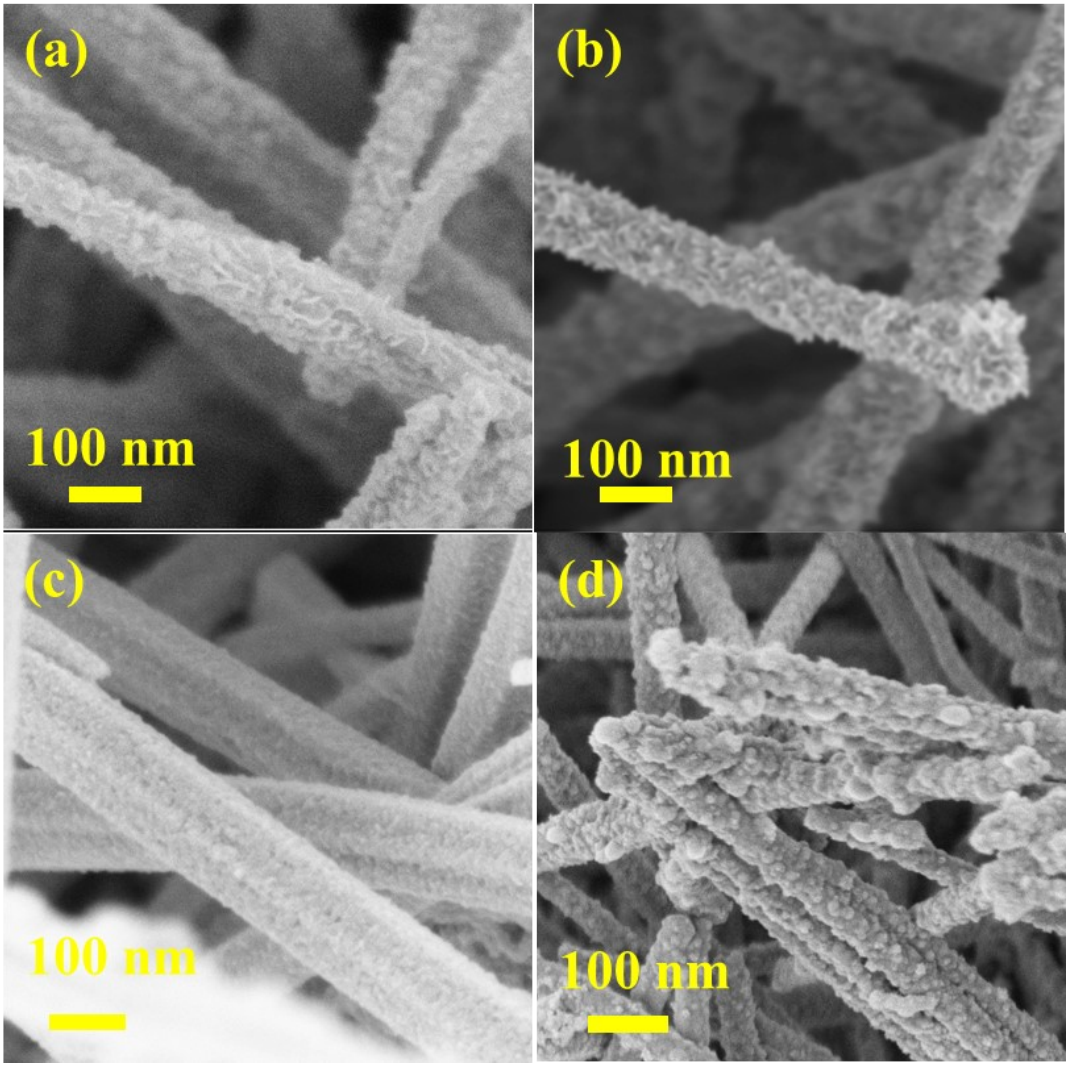

Fig. S1 FE-SEM image of as-synthesized (a) Co_9S_8@MoSe, (b)Co_9S_8@$Ni_{0.5}Mo_{0.5}$-Se, (c)Co_9S_8@$Ni_{0.25}Mo_{0.75}$-Se and Co_9S_8 @$Ni_{0.75}Mo_{0.25}$-Se.

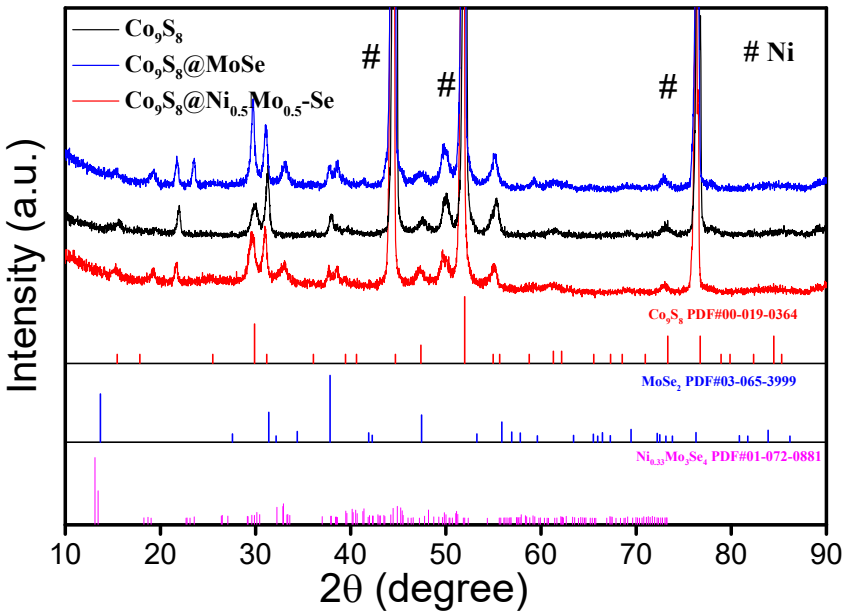

Fig. S2. XRD spectrum of as-synthesized Co_9S_8, Co_9S_8@MoSe, and Co_9S_8@$Ni_{0.5}Mo_{0.5}$-Se.

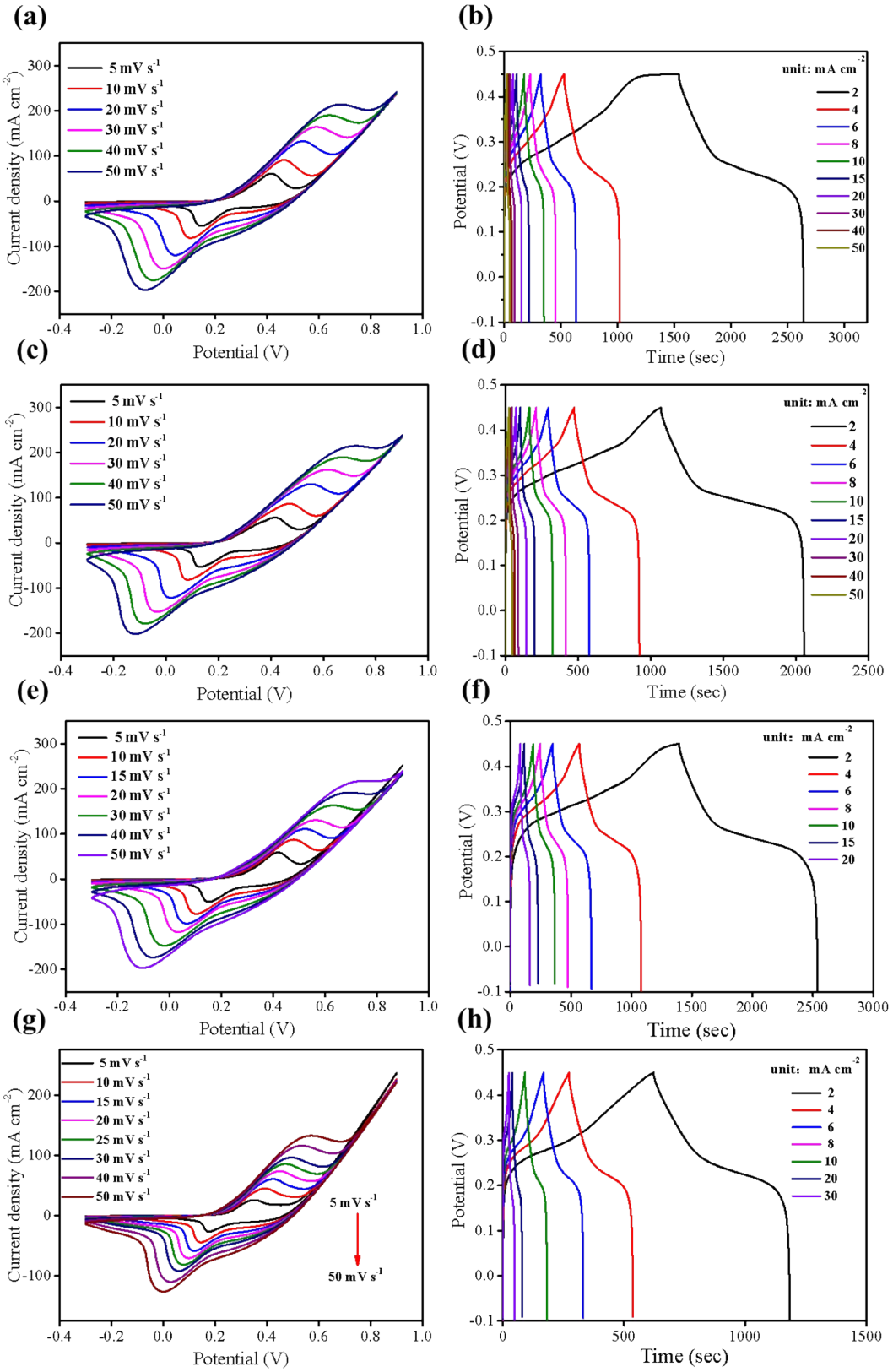

Fig. S3. CV and GCD curves of: (a-b) Co_9S_8@$Ni_{0.25}Mo_{0.75}$-Se, (c-d) Co_9S_8@$Ni_{0.75}Mo_{0.25}$-Se, (e-f) Co_9S_8@MoSe, (g-h) bare Co_9S_8.

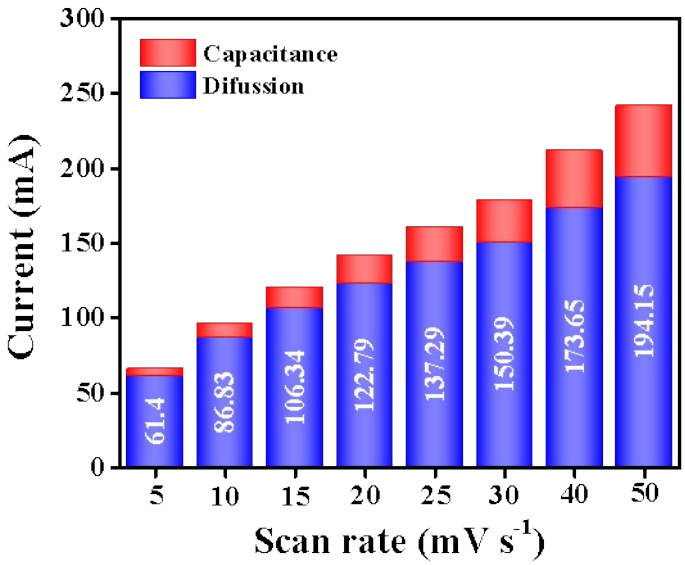

Fig. S4. Surface-controlled and diffusion controlled capacity contribution of $Co_9S_8@Ni_{0.5}:Mo_{0.5}$-Se

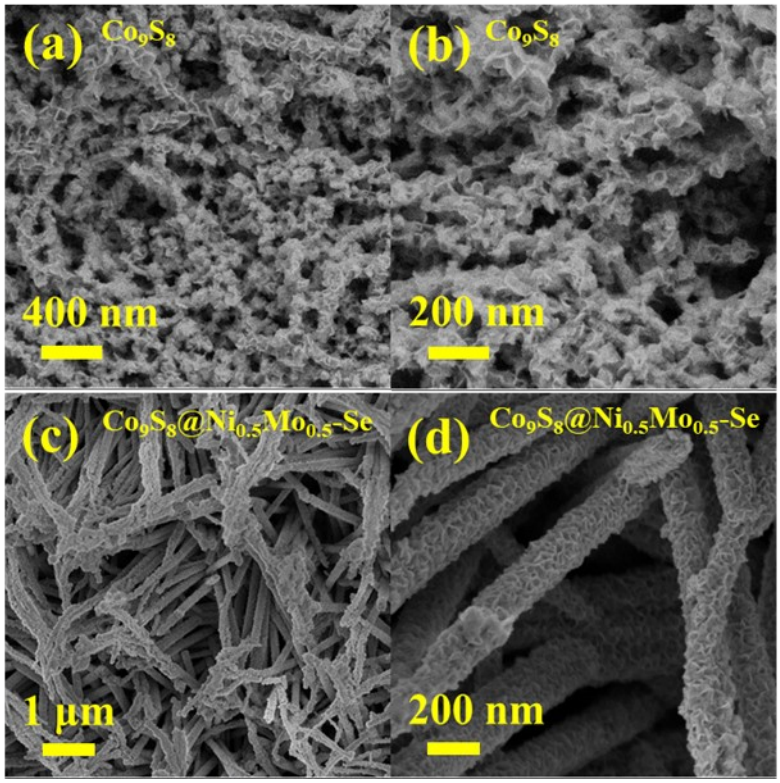

Fig. S5. FE-SEM image of Co_9S_8 NWs (a-b) and $Co_9S_8@Ni_{0.5}$ $Mo_{0.5}$–Se NWAs(c-d) after the cycling test

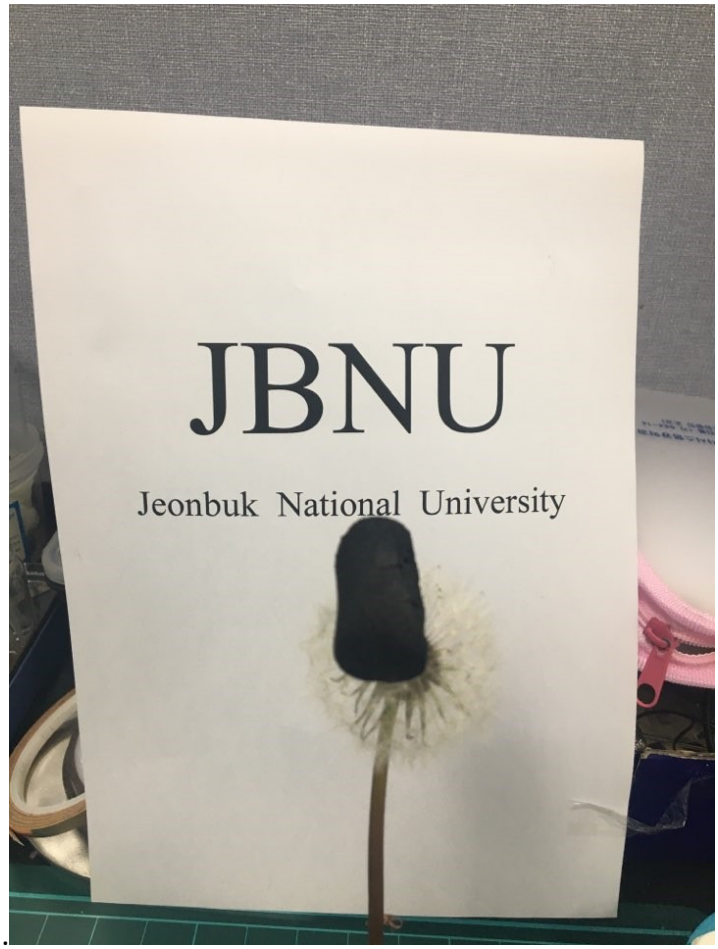

Fig. S6. Digital photograph of a cylindrical shape Fe_2O_3@PANNFs/N-rGO aerogel held free-standing on the top of a dandelion demonstrating its ultra-lightness.

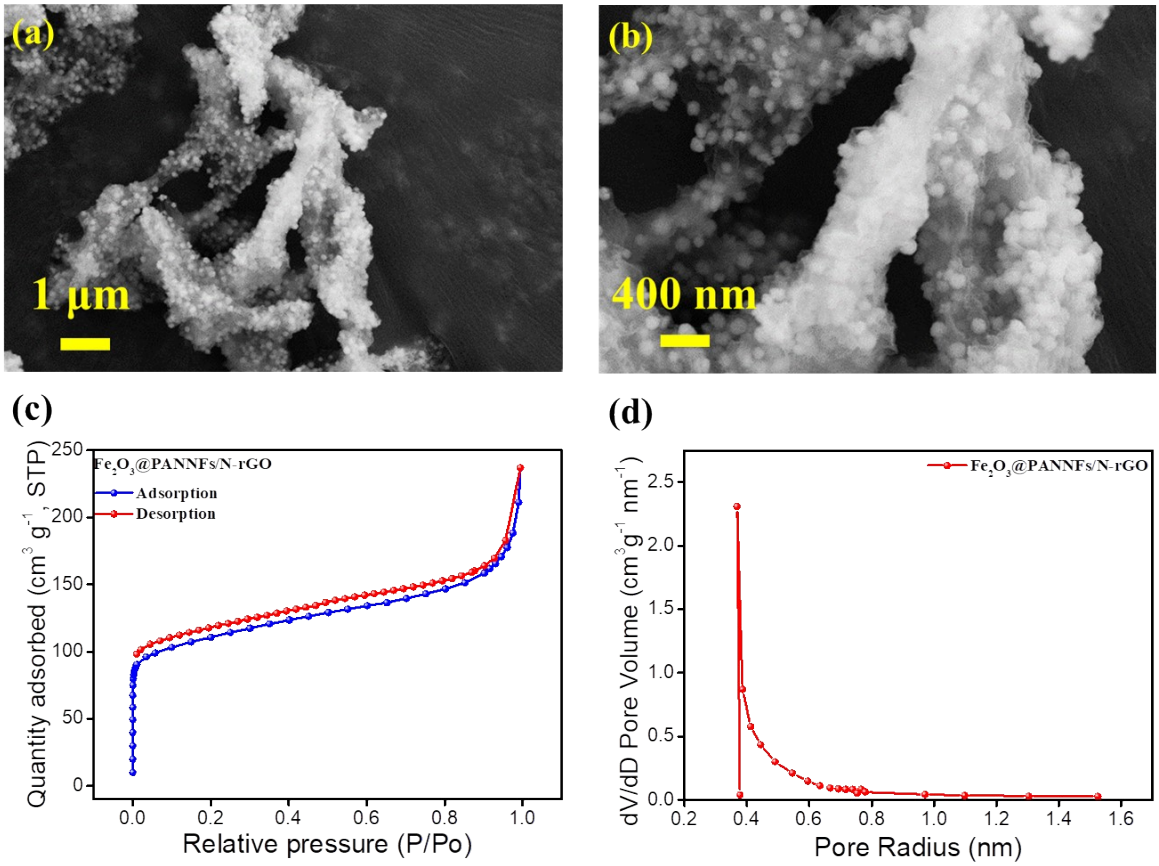

Fig. S7. (a, b) FE-SEM of Fe_2O_3@PANNFs/N-rGO at different magnifications, (c) N_2 sorption isotherms, and (d) pore size distribution of the Fe_2O_3@PANNFs/N-rGO.

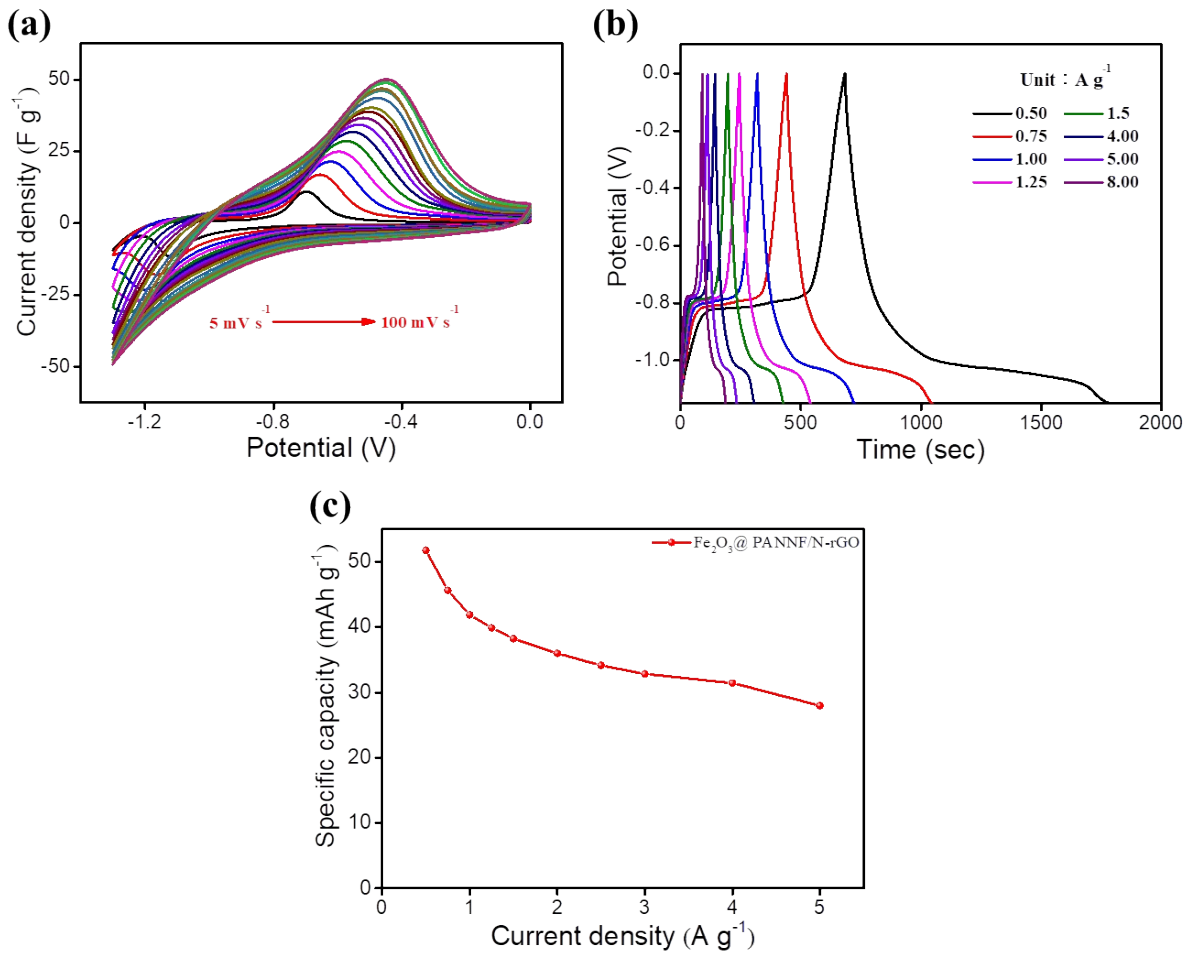

Fig. S8. (a) CV curves of the Fe_2O_3@PANNFs/N-rGO at different scan rate. (b) The GCD curves of the Fe_2O_3@PANNFs/N-rGO at different current density. (e) The specific capacity vs. current density of Fe_2O_3@PANNFs/N-rGO;

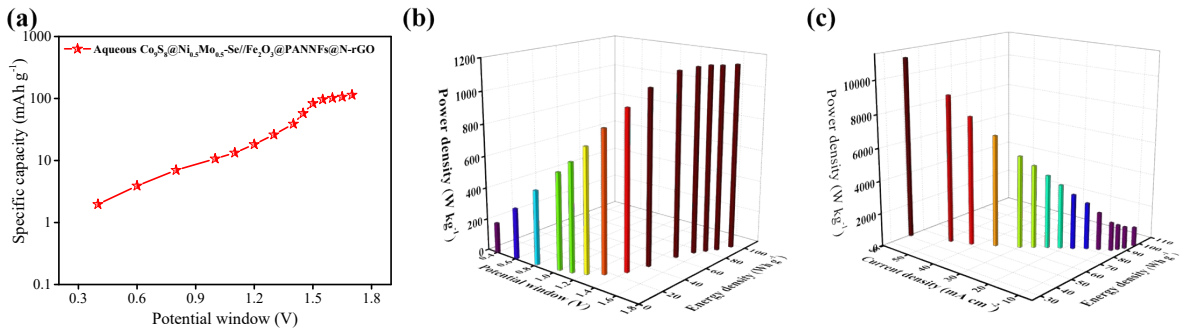

Fig. S9. (a) The specific capacity vs. operating voltage windows of Co_9S_8@Ni-Mo-Se//Fe_2O_3@PANNFs/N-rGO ASC. (b) 3D Bar plots (energy density vs. power density vs. operating voltage windows) of Co_9S_8 @ Ni-Mo-Se//Fe_2O_3@ PANNFs/N-rGO aqueous ASC. (c) 3D Bar plots (energy density vs. power density vs. current density) of Co_9S_8@Ni-Mo-Se//Fe_2O_3@PANNFs/N-rGO aqueous ASC

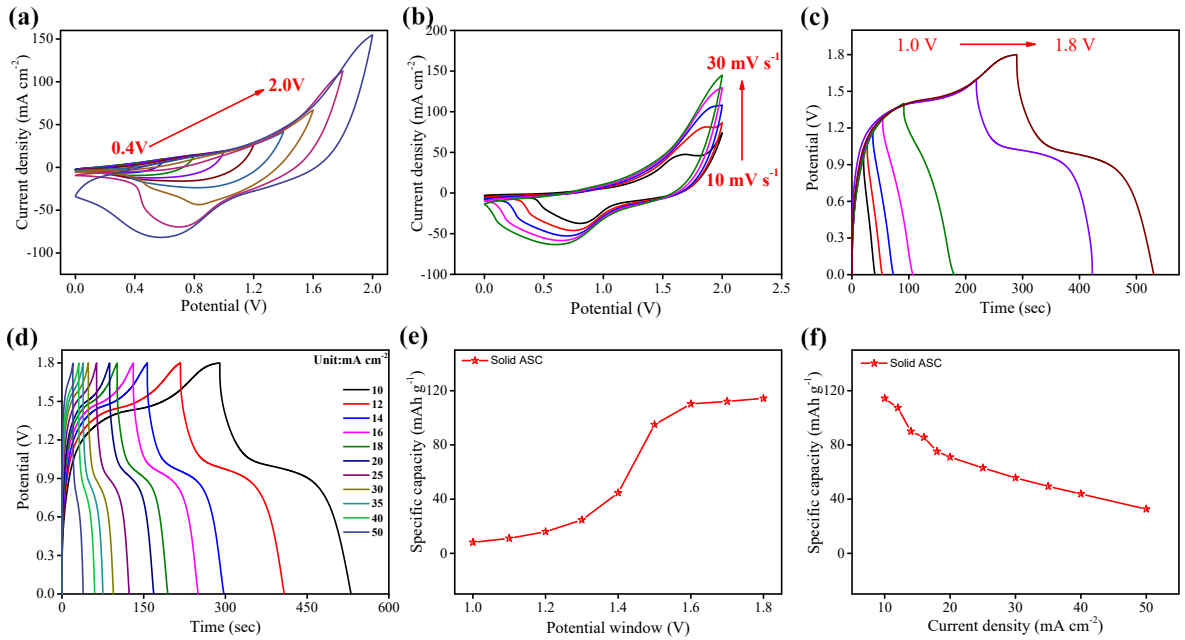

Fig. S10. (a) CV curves (scan rate 50 mV s^{-1}) of all-solid-state Co_9S_8@$Ni_{0.5}Mo_{0.5}$-Se//Fe_2O_3@PANNFs/N-rGO ASC at various operating voltage windows. (b) CV curves of all-solid-state Co_9S_8@$Ni_{0.5}Mo_{0.5}$-Se//Fe_2O_3@PANNFs/N-rGO ASC at various sweep rates from 10–50 mV s^{-1}. (c) GCD curves of all-solid-state Co_9S_8@$Ni_{0.5}Mo_{0.5}$-Se//Fe_2O_3@PANNFs/N-rGO aqueous ASC at various operating voltage windows. (d) The specific capacity vs. perating voltage windows of Co_9S_8@$Ni_{0.5}Mo_{0.5}$-Se//Fe_2O_3@PANNFs/N-rGO aqueous ASC. (e) GCD curves of all-solid-state Co_9S_8@$Ni_{0.5}Mo_{0.5}$-Se//Fe_2O_3@PANNFs/N-rGO ASC at various current densities from 10 to 50 mA cm^{-2}. (f) The specific capacity vs. current density of all-solid-state Co_9S_8@$Ni_{0.5}Mo_{0.5}$-Se // Fe_2O_3@PANNFs/N-rGO ASC;

Table S1. Electrode properties comparison with reported literatures.

Electrode Materials	Areal Capacitance / capacity	Specific capacitance /capacity	Current load	Electrolyte	Stability (Cycles)	Ref.
$CoNi_2S_4$/SNGA	-	318.3 mAh g^{-1}	1 A g^{-1}	6 M KOH	95.8% (10000)	[6]
Ni-Co-S/G	-	1492 F g^{-1}	1 A g^{-1}	6 M KOH	90% (8000)	[7]
VACNTF@MoSe	-	435 F·g^{-1}	1 A g^{-1}	2 M KOH	92% (5000)	[8]
$MoSe_2$/graphene Nanosheet	-	945 F·g^{-1}	1 A g^{-1}	6 M KOH	92% (2000)	[9]
CoSe Nanosheet	-	70.6 mAh g^{-1}	1 A g^{-1}	2M KOH	-	[10]
NiSe@$MoSe_2$ Nanosheet	-	128.2 mAh g^{-1}	1 A g^{-1}	2 M KOH	93.7% (1000)	[11]
$CoSe_2$/$Ni_{0.85}Se$ Nanotube	-	171 mAh g^{-1}	1.9 A g^{-1}	6 M KOH	95.3% (6000)	[12]
$MoSe_2$-$Ni(OH)_2$ Nanosheet	-	146.9 mAh g^{-1}	1 A g^{-1}	6 M KOH	90% (3000)	[13]
$CoSe_2$/$MoSe_2$ Hollow Nanosphere	-	211.97 mAh g^{-1}	1 A g^{-1}	3 M KOH	94.2% (2000)	[14]
Co-Mo-Se Nanosheet arrays	-	221.7 mAh g^{-1}	1 A g^{-1}	6 M KOH	95% (8000)	[15]
Ni_3S_2@PPy	3148 mF cm^{-2}	-	2 mA cm^{-2}	2 M KOH	91.2% (4000)	[16]
Ni_3S_2–$Cu_{1.8}S$ NS	-	1686 F g^{-1}	1 A g^{-1}	2 M KOH	88.94% (10000)	[17]
$ZnCo_2O_4$	3.07 F·cm^{-2}	-	1.04mA cm^{-2}	6 M KOH	78.85% (3000)	[18]
peptide-Co_9S_8	1300 mF cm^{-2}	1800 F g^{-1}	0.7mA cm^{-2}	1 M KOH	96% (5000)	[19]
MnO_2@Co_9S_8/NF	-	643.3 C g^{-1}	3 mA cm^{-2}	3 M KOH	120% (10000)	[20]
Co_9S_8@PPy@NiCo-LDH	2.65 F cm^{-2}	-	1 mA cm^{-2}	1 M LiOH	88.67% (10000)	[21]
Co_9S_8@Ni-MoSe core-shell NWAs	**0.93 mAh cm^{-2}**	**460.81mAh g^{-1}**	**1.5 mA cm^{-2}**	**2 M KOH**	**94.3% (10000)**	**This work**

Table S2. ASCs device properties comparison with reported literature

Reported ASC Device	Energy density (Wh kg^{-1})	Power density (W kg^{-1})	Device Window (V)	Electrolyte	Stability (Cycles)	Ref.
$NiCo_2S_4$//G/C	42.3	476	0-1.6	6 M KOH	78.6% (10000)	[7]
Ni-Co-S/G//PCNS	43.3	800	0-1.6	6 M KOH	85% (10000)	[6]
$FeCo_2S_4$//3D PNG	76.1	755	0-1.6	KOH/PVA	82% (10000)	[23]
$CoMoS_4$//rGO	27.2	400	0-1.6	1 M KOH	86% (10000)	[22]
$CoSe_2/MoSe_2$-3-1//AC	51.84	799.2	0-1.6	3 M KOH	93.4% (10000)	[14]
$MoSe_2$-$Ni(OH)_2$//AC	43	817	0-1.6	6 M KOH	85% (5000)	[13]
E-$CoSe_2/Ni_{0.85}Se$//AC	40.5	538	0-1.6	6 M KOH	82% (5000)	[12]
NiSe@$MoSe_2$//N-PMCN	32.6	415	0-1.65	2M KOH	91.4% (5000)	[11]
CoSe//AC	18.6	750	0-1.5	2M KOH	95.4% (20000)	[10]
Co–Mo–Se//AC	44.7	1094	0-1.55	KOH/PVA	90.7% (8000)	[15]
MnO_2@Co_9S_8//AC	35	240	0-1.6	3M KOH	97.5% (36000)	[20]
Co_9S_8@Ni-MoSe //Fe_2O_3@PAN NFs@ N-rGO	**96.9**	**1158**	**0-1.7**	**PVA/ KOH**	**94.47% (10000)**	**This work**

Reference

[1] J. Balamurugan, T. D. Thanh, N. H. Kim, J. H. Lee, Adv. Mater. Interfaces, 2016, **3**, 1500348.

[2] Y. Ruan, L.Lv , Z. Li , C. Wang and J. Jiang, 2017, **9**, 18032.

[3] J. Balamurugan, C. Li, V. Aravindan, N. H. Kim, and J.H. Lee, Adv. Funct. Mater., 2018, **28**, 1803287.

[4] Y. Al Haj, J. Balamurugan, N. H. Kim and J. H. Lee, J. Mater. Chem. A, 2019, **7**, 3941

[5] M. Guo, J. Balamurugan, T. D. Thanh, N. H. Kim and J. H. Lee, J. Mater. Chem. A, 2016, **4**, 17560

[6] G. J. He, M. Qiao, W. Y. Li, Y. Lu, T. T. Zhao, R. J. Zou, B. Li, J. A. Darr, J. Q. Hu, M. M. Titirici, I. P. Parkin, Adv. Sci., 2017, **4**, 1600214.

[7] J. Yang, C. Yu, X. Fan, S. Liang, S. Li, H. Huang, Z. Ling, C. Hao, J. Qiu, Energy Environ. Sci., 2016, **9**, 1299.

[8] Y.H. Liu, W.L. Li, X.W. Chang, H. Chen, X.L. Zheng, J.B. Bai, Z.Y. Ren, J. Colloid Interface Sci., 2020, **562**, 483-492.

[9] B. Kirubasankar, S. Vijayan, S. Angaiah, Sustainable Energy Fuels, 2019, **3**,467-477.

[10] Y.R. Zhu, Z.D. Huang, Z.L. Hu, L.J. Xi, X.B. Ji, Y. Liu, Electrochim. Acta, 2018, **269**,30-37.

[11] H. Peng, J.Z. Zhou, K.J. Sun, G.F. Ma, Z.G. Zhang, E. Feng, Z.Q. Lei, ACS Sustainable Chem. Eng., 2017, **5**, 5951-5963.

[12] J.H. Lin, H.H. Wang, Y.T. Yan, X.H. Zheng, H.N. Jia, J.L. Qi, J. Cao, J.C. Tu, W.D. Fei, J.C. Feng, J. Mater. Chem. A, 2018, **6**, 19151-19158.

[13] B. Kirubasankar, P. Palanisamy, S. Arunachalam, V. Murugadoss, S. Angaiah, Chem. Eng. J., 2019, **355**, 881-890.

[14] F. Ma, J. Lu, L. Pu, W. Wang, Y. Dai, J. Colloid Interface Sci.,2020, **563**, 435-446.

[15] C. Miao, C. Zhou, H. Wang, K. Zhu, K. Ye, Q. Wang, J. Yan, D. Cao, N. Li, G. Wang, J. Power Sources 2021, **490**, 229532

[16] J. Ren, M. Shen, Z.Li, C. Yang, Y. Liang, H.Wang, J. Li, N. Li, D. Qian, J. Power Sources 2021, **501**, 230003;

[17] Y. Liu , G. Liu , X. Nie , A. Pan, S. Liang, and T. Zhu, J. Mater. Chem. A, 2019, **7**, 11044-11052

[18] J. Zhu, D.Song, T. Pu, J. Li, B. Huang, W. Wang, C. Zhao, L. Xie, L. Chen,Chem. Eng. J., 2018, **336**, 679-689

[19] W. Xiong, K. Hu, Z.Li, Y. Jiang, Z. Li, Z. Li, X. Wang, Nano Energy, 2019, **66**,104149.

[20] Q. Hu, X. Jiang, M.He, Q. Zheng, K. H. Lam, D. Lin, Electrochim. Acta, 2020, **338**,135896.

[21] L. Wang, S. Li, F. Huang, X. Yu, M. Liu, H. Zhang, J. Power Sources, 2019, **439**, 227103.

[22] X. Y. Xu, Y. H. Song, R. N. Xue, J. K. Zhou, J. P. Gao, and F. B. Xing, Chemical. Engineering Journal, 2016, **301**, 266.

[23] S. Tang, B. Zhu, X. Shi, J. Wu, and X. Meng, Adv. Energy Mater., 2017, **7**, 1601985.